ISSN Print: 2394-7500
ISSN Online: 2394-5869
Impact Factor (RJIF): 8.69
IJAR 11(10): 342-352
www.allresearchjournal.com
Received: 02-07-2025
Accepted: 05-08-2025

Kum Dong Hong
Faculty of Metallic Engineering, Kim Chaek University of Technology, Pyongyang, Democratic People's Republic of Korea

Ju Song Kim
Faculty of Metallic Engineering, Kim Chaek University of Technology, Pyongyang, Democratic People's Republic of Korea

Yong Song Pak
Faculty of Metallic Engineering, Kim Chaek University of Technology, Pyongyang, Democratic People's Republic of Korea

Corresponding Author:
Kum Dong Hong
Faculty of Metallic Engineering, Kim Chaek University of Technology, Pyongyang, Democratic People's Republic of Korea

Hydrodynamic analysis to determine the optimum structural dimensions of a dechlorinated stirrer in a wet zinc sublimation process

Kum Dong Hong, Ju Song Kim and Yong Song Pak

DOI: https://www.doi.org/10.22271/allresearch.2025.v11.i10e.12957

Abstract
In this paper, the optimum structural dimensions of a reaction stirred tank were determined to further enhance the cleaning effect of impurity chloride ions in a wet process for the production of electrolytic zinc from zinc sublimates. Chloride ions contained in the leachate are removed by the addition of copper powder, while the cleaning effect is determined by the distribution of copper powder in the stirrer. For the determination of the optimum structural dimensions, the hydrodynamic analysis was carried out using Fluent 17.1. The standard k-e model was used as the viscous model in the multi-reference system, the silmon model as the turbulent dissipative force model and the Gidaspow model as the interfacial drag force model with the model developed in Solidworks 2018. Using this model, the optimum structural dimensions of the impeller were determined, with the best effect of chlorine cleaning in the impeller when the impeller diameter was 1.0 m, height 1.5 m, baffle size 0.2×0.9×0.01 m, baffle size four symmetrically, impeller diameter 0.4 m, impeller diameter 60 mm, impeller angle 45°, bed height 0.225 m, rotational speed 150 rpm, and clockwise rotation.

Keywords: Dechlorinate, hydrodynamic analysis of stirred tank, purification of chlorine ion, optimum structure of agitator

1. Introduction
Zinc sublimation includes zinc leaching residue, rotary furnace sublimation from the converter volatilization process of zinc oxide ore, fusing furnace sublimation from the lead smelting process, dust from smelting of scrap brass, and steelmaking dust (zinc content about 20%) from the recovery of galvanized scrap.

In many literatures [4, 5, 7], the composition of zinc sublimates, one of the main characteristics of zinc sublimates, is described to vary greatly depending on the nature of the starting material. For example, rotary kiln oxides contain a considerable concentration of Zn, Pb, Cd and dispersed rare metals compared to the starting materials, MgO, CaO, Al_2O_3, SiO_2, C, organic matter that are mechanically transferred with rotary kiln gases, and SO_2 gas adsorbed on the surface.

The composition of zinc sublimates is shown in Table 1.1 [5-7]. As shown in Table 1, sublimates are complex in composition and have a relatively high impurity content. Therefore, sublimates are usually leached separately to obtain a clean $ZnSO_4$ solution and then sent to the hydro-zinc metallurgical quenching leaching system to be treated together.

Table 1: Composition of several zinc sublimates, wt%

Element sublimate	Zn	Pb	Cd	Cu	S	Fe	As	SiO_2	Sb	Cl	F
1	56.7	14.5	1.02	0.23	4.6	1.3	0.16	24	0.04	0.1	0.05
2	40.4	14.3	0.46	0.03	4.05	7.31	0.03	6.4	-	-	-
3	67	4.3	0.52	0.62	3.4	0.73	-	1.0	-	0.25	-
4	61.1	12.5	0.6	0.22	2.98	2.01	0.71	2.96	0.04	0.32	-

Zinc sublimates usually contain many impurities, e.g. F, Cl, As, Sb, which are harmful to zinc electrolysis, and F and Cl contents are 2-10 times higher than zinc quenching and As

and Sb contents are higher than quenching. Meanwhile, sublimates contain disperse rare metals such as In, Ge, and Ga. Especially, it is very difficult to avoid the negative effects of F and Cl in sublimates when they are transferred to solution during the wet treatment of sublimates. Therefore, zinc sublimates must be pretreated before leaching. During dilute sulfuric acid leaching of zinc sublimates, the chlorine leached into solution is removed by the addition of silver sulfate or copper chloride. In this context, silver sulfate is not widely used in the treatment of high-chlorine zinc feedstock due to its high reagent cost.
The chlorine removal in zinc sulfate solution by cupric chloride was carried out by adding a certain amount of copper powder at pH ~4, initial copper concentration of 400 mg/L and temperature of 50 °C. This reaction was carried out under stirring conditions, so that the reaction time and chlorine removal rate were determined according to the stirring characteristics of the stirrer. It is therefore very important to characterize the dispersion of solid particles in the liquid and, on this basis, to determine the optimum structure and size of dechlorination stirrer which can maximize the efficiency.

2. Mathematical Modeling and Boundary Conditions Setting

The aim of stirring is to maximize the reaction rate by maximizing the effect of contact with the leachate by flotation and movement of copper powder in a stirred tank. Therefore, its interaction is referred to as the liquid-solid phase interaction as the process of interaction of the particle with the leachate.
We make the following assumptions to study the liquid-solid phase interaction by stirring.
First, the stirring process is a liquid-solid interaction, neglecting the gas-phase interaction, such as air and gas generation.
Second, chemical reactions are not considered, taking into account the stability and time of the solution during stirring.
Third, fluid flow is considered turbulent because of incompressible and high Reynolds number.
Fourth, the small size inside the particle makes it unlikely that heat and mass transfer by diffusion is present.
Based on the previous work [11-16], the governing equations, viscosity equations, turbulent dissipation force models and interface resistance equations were chosen and the geometrical dimensions and boundary conditions were set.

2.1 Mathematical Models

2.1.1 Governing Equations

The Euler-Euler multiphase model was used for the hydrodynamic simulation of the slurry. In this model, the phase is treated as an interpenetrating continuum, expressed as a volume fraction at each point of the system. The Reynolds-averaged mass equation and momentum balance equation can be solved for each phase [1-3, 18-20].
Continuity equation:

$$\frac{\partial}{\partial t}(\alpha_q\rho_q) + \nabla.(\alpha_q\rho_q\vec{u}_q) = 0 \qquad (1)$$

Momentum equation:

$$\frac{\partial}{\partial t}(\alpha_q\rho_q\vec{u}_q) + \nabla.(\alpha_q\rho_q\vec{u}_q\vec{u}_q) = -\alpha_q\nabla P + \nabla.\bar{\bar{\tau}}_q + \alpha_q\rho_q\vec{g} + +(\vec{F}_{td} + \vec{F}_q + \vec{F}_{lift,q} + \vec{F}_{vm,q}) + \vec{F}_{12} \qquad (2)$$

where q is denoted by 1 or 2 as the primary and secondary phases, respectively.
α is the volume fraction, ρ is the density, $\vec{u}$ is the velocity vector, and P is the pressure, which is divided by the two phases.

- $\bar{\bar{\tau}}$;the stress tensor due to viscosity and velocity fluctuations,
- g; gravity,
- $\vec{F}_{td}$; force,
- $\vec{F}_{vm,q}$; virtual mass force,
- $\vec{F}_{12}$; interfacial interaction force.

The rotation of the impeller is simulated using a multi-reference frame (MRF) [20, 21, 22].

2.1.2 Viscosity Model [3]

The standard k-e model was used as the viscous model.

$$\frac{\partial}{\partial}(\rho_m k) + \nabla.(\rho_m k\overrightarrow{u_m}) = \nabla.\left(\frac{\mu_{t,m}}{\delta_k}\nabla k\right) + G_{k,m}\text{-}\rho_m\varepsilon \qquad (3)$$

$$\frac{\partial}{\partial}(\rho_m\varepsilon) + \nabla.(\rho_m\varepsilon\overrightarrow{u_m}) = \nabla.\left(\frac{\mu_{t,m}}{\delta_k}\nabla\varepsilon\right) + \frac{1}{k}\left(C_{1,\varepsilon}G_{k,m} - C_{2,\varepsilon}\rho_m\varepsilon\right) \qquad (4)$$

$C_{1\varepsilon}$and $C_{2\varepsilon}$are constants, σk and σεare turbulent Plant constants.
The mixture density ρm and velocity $\overrightarrow{u_m}$ are calculated by the following equation:

$$\rho_m = \sum_{i=1}^{N}\alpha_i\rho_i \qquad (5)$$

$$\overrightarrow{u_m} = \sum_{i=1}^{N}\alpha_i\rho_i\overrightarrow{u_i} / \sum_{i=1}^{N}\alpha_i\rho_i \qquad (6)$$

2.1.3 Turbulent Dissipative Forces [1, 3].

The turbulent fluctuations result in the dispersion of phases in the region of large volume fraction to the region of small volume fraction. The turbulent dissipation force is significant when the size of the turbulent vortex is larger than the particle size.
The effect of turbulent dissipation force on the hydraulic properties in the leaching tank is investigated using the Silmon model. The model equation of turbulent dissipation force is

$$\overrightarrow{F_{td,q}} = C_{TD}K_{pq}\frac{D_{t,q}}{\delta_{pq}}\left(\frac{\nabla\alpha_p}{\alpha_p} - \frac{\nabla\alpha_q}{\alpha_q}\right) \qquad (7)$$

2.1.4 Interfacial Resistance Forces [2, 3]

The results of the previous studies used Schillar Nauman resistance model, Gidaspow model, Wen and Yu model, Brucato model, etc.
We used the Gidaspow model.

$$F_d = \frac{3\alpha_i\alpha_s\rho_i C_D}{4d_p V^3}R_e(\overrightarrow{u_l} - \overrightarrow{u_s}) \qquad (8)$$

The particle-particle collision coefficient was set to 0.98.

2.2 Geometric Model and Boundary Conditions Selection

2.2.1 Geometric Modeling

The geometry model was created in SolidWorks software and was called the Design Modeler of ANSYS Workbench.
The geometry created a circular stirrer tank with four baffles and flat bottom, and the blade was created as a single-stage

two-blade. We also created a rotating region 1.1 times the blade diameter.
The geometry created is shown in Fig. 1.

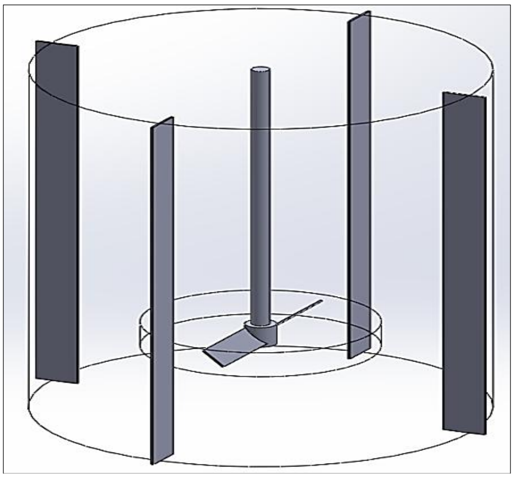

Fig 1: Geometric model for simulation

The created geometry was imported into Meshing of ANSYS Workbench to perform mesh. The mesh used the full mesh control, where sizing/Relevance Center was chosen as Fine, Smoothing as Medium, and Curvature Nomal Angle as 18°. The mesh model is tetrahedral. The number of elements is 465253 and the number of nodes is 94707.
The mesh model is shown in Fig. 2.

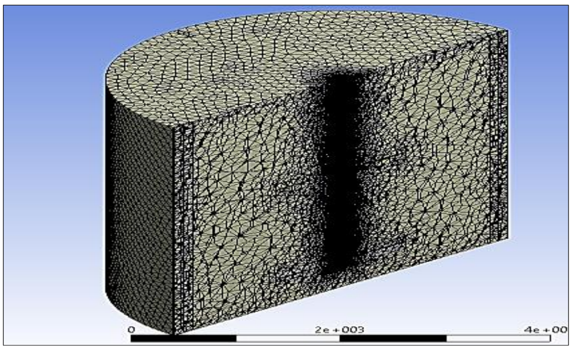

Fig 2: Meshing model

2.2.2. Setting boundary conditions

The setting of boundary conditions has a great influence on the accuracy of the simulation results.
The boundary conditions are defined by the results of the previous work as follows :

1. The impeller is treated using the MRF method.
   The rotational speed of the rotating zone and the impeller are the same. In the static region, the fluid flow is at rest.
2. The impeller is set to a moving wall (Moving Wall).
   Then the blade velocity becomes zero for the fluid in the rotating region.
   The stirred tank wall is set to a static wall (Stationary Wall).
3. The interface between the rotating and static regions is defined as interface boundary conditions.
4. The top of the stirred tank is assumed to be open and set to zero shear wall.

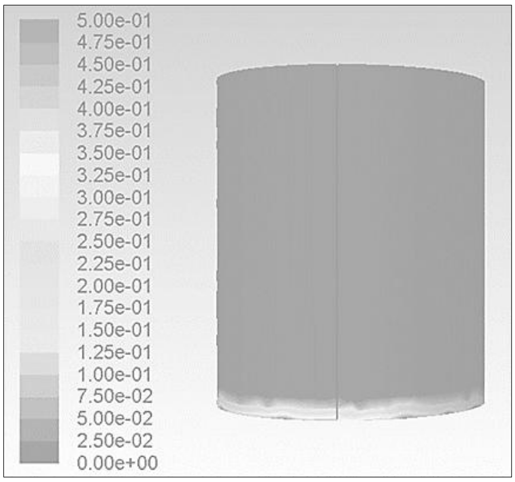

Fig 3: Phase-fraction contours patched with solid and liquid phases

It is assumed that the solid particles in the stirred tank are set at the beginning of the simulation.
Therefore, a solid volume fraction of 0.5 was set to 0.5 as the solid volume fraction and patched to the top 30 mm below the stirrer height as the solid dispersed throughout the stirrer.
The results obtained by Patch are shown in Fig. 3.
To form a turbulent model, we use the standard k-e model.
The model parameters are Cμ:0.09, Cs:0.22, C1:1.8, C2:0.6, C1ε:1.44, C2ε:1.92, σk:1.0, σε:1.3.
The solution scheme is used with the SIMPLE scheme with standard pressure interpolation.
To avoid numerical divergence and non-physical oscillations, the QUICK discretization scheme was used to calculate the momentum, volume fraction, turbulent kinetic energy, and turbulent loss rate.
The convergence of the simulation was verified by controlling not only the residual values but also additional parameters such as turbulence loss over the volume, turbulence loss at the lower surface of the blade, and torque at the shaft.
Fixing the residual and additional parameters, the simulation is well converged.
We used ANSYS Fluent 17.1 as a program to simulate the steady-state process.

3. CFD simulation analysis for rational design of dechlorination stirrer

The optimum design parameters of dechlorination stirrer were determined by considering the effects of design parameters such as the direction of impeller rotation, the position of impeller installation and the number of cycles on the flotation characteristics of solid particles.

3.1 Effect of the impeller rotation direction on the flotation characteristics and stirring effect of solid particles

The geometry of the model set is shown in Table 2.

Table 2: The geometry of the stirrer tank model

№	Geometric indices	value
1	H, mm	1 500
2	D, mm	1 000
3	d, mm	0.4D
4	C_1, mm	0.1H

Table 2. The geometry of the stirrer tank model

Also, the stirring speed and material properties values are shown in Table 3.

Table 3: Speed of agitation and material properties

N(r/min)	ρ_l(kg/m^3)	μ_l(Pa·s)	ρ_s(kg/m^3)	d(mm)
120	1100	0.001	8960	0.074

The fluid flow characteristics were evaluated when the impeller was rotated counterclockwise and counterclockwise at 120 rpm (Fig. 4).

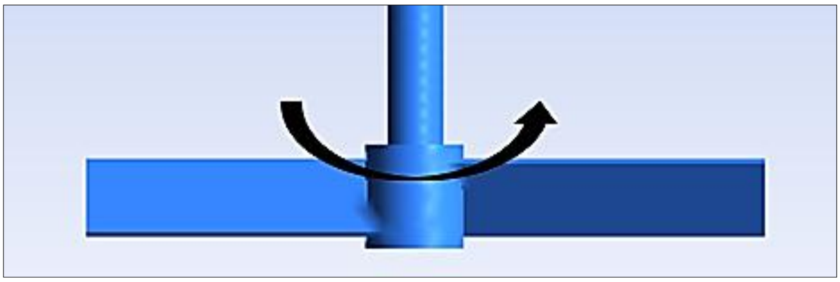

Fig 4: The direction of rotation of the impeller (counterclockwise)

The simulation results are shown in Figs. 5 and6. As shown in Fig. 5a, the velocity vector is symmetrical about the axis, forming a circulating flow throughout the stirred tank. That is, the solid particles, which are subjected to the rotating force of the impeller, flow downward and accelerate against the wall, and flow upward with a large force and a fast velocity, forming a circulation loop.

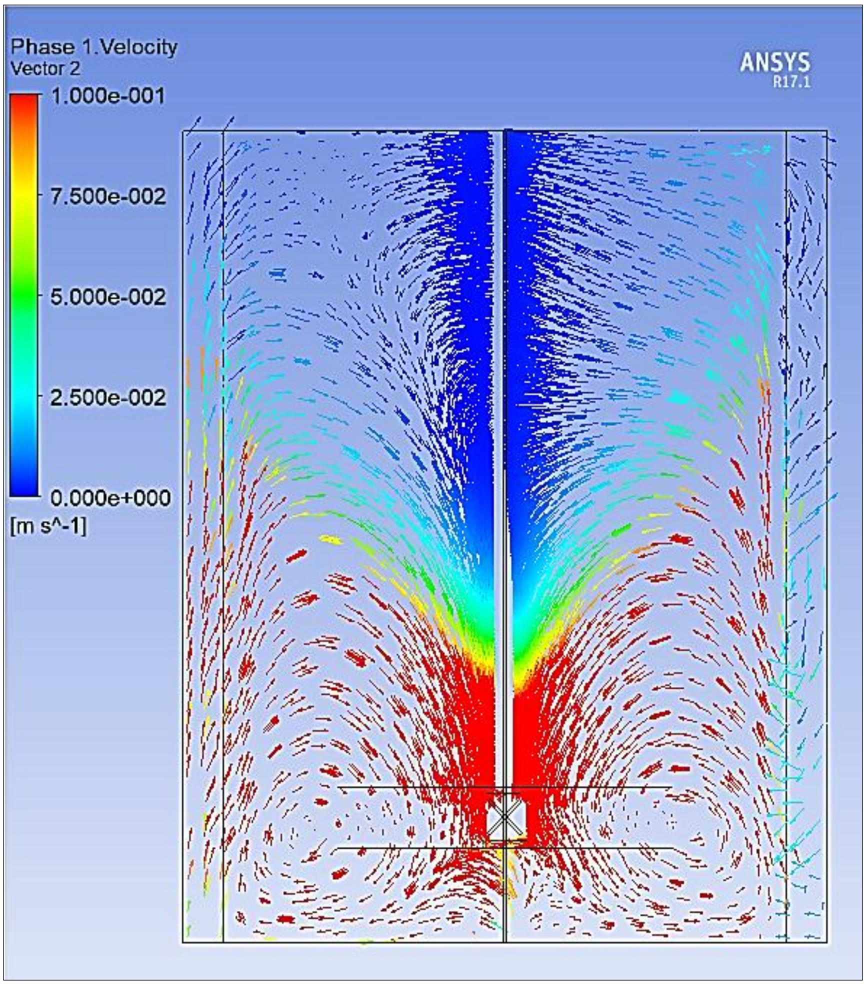

a) Distribution of Velocity vector

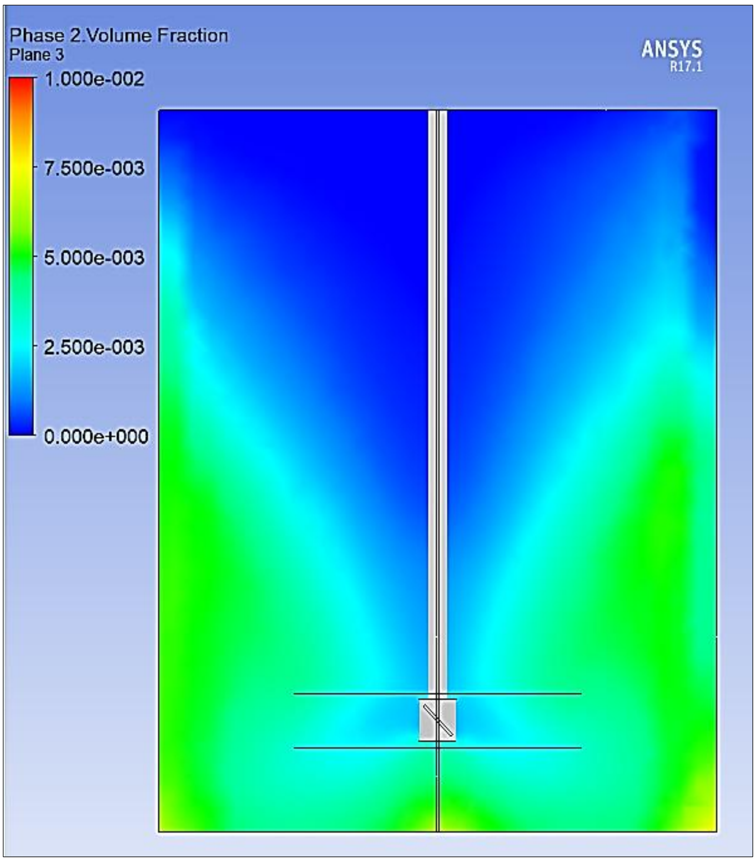

b) Volume fraction distribution of solid particles

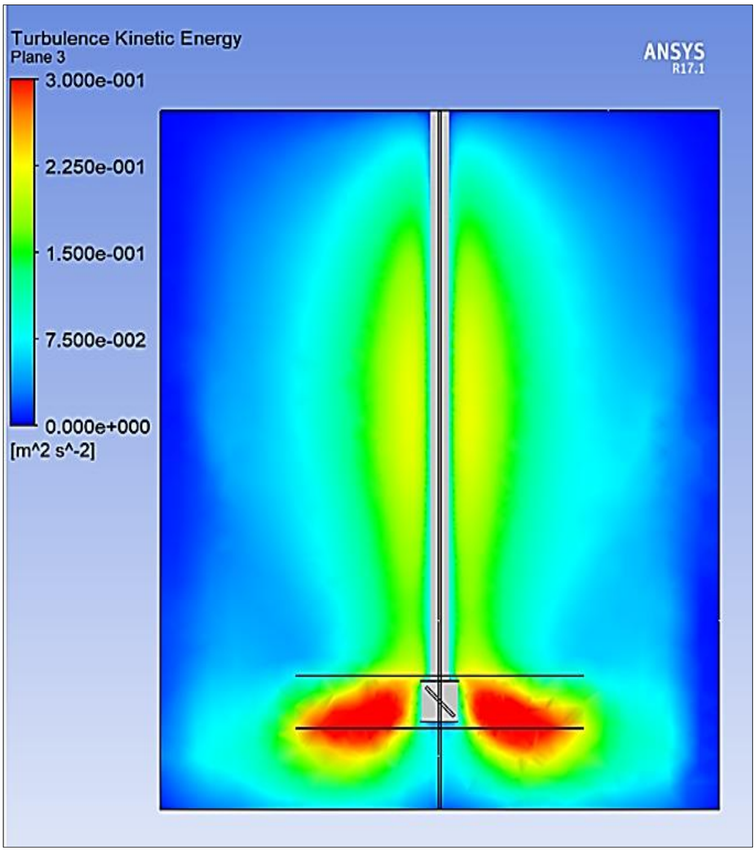

c) Turbulent kinetic energy distribution

Fig 5: Simulation results of clockwise rotating impeller

In Fig. 5a, the velocity vector is symmetrical about the axis, forming a small circulating flow in the stirred tank. It is observed that the particles forced by the impeller rise in the inclination angle and when they collide with the wall, they split into two opposite streams, forming two loops.

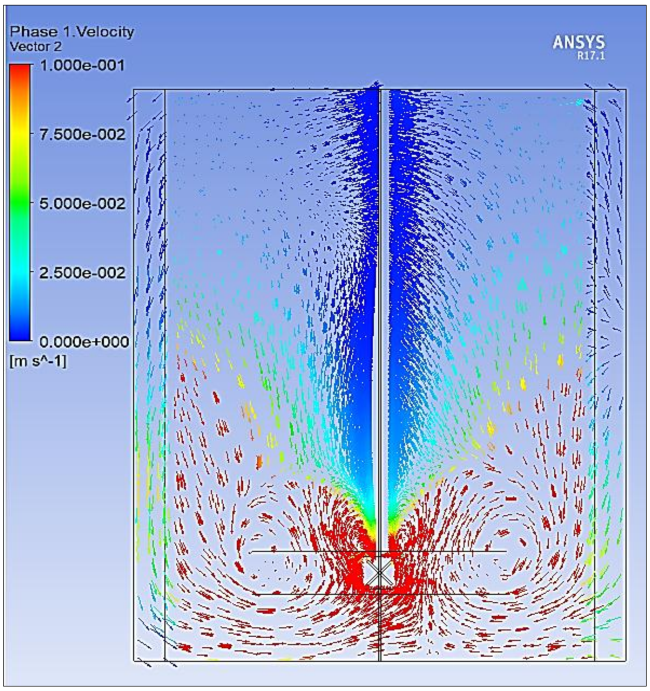

a) Velocity vector distribution diagram

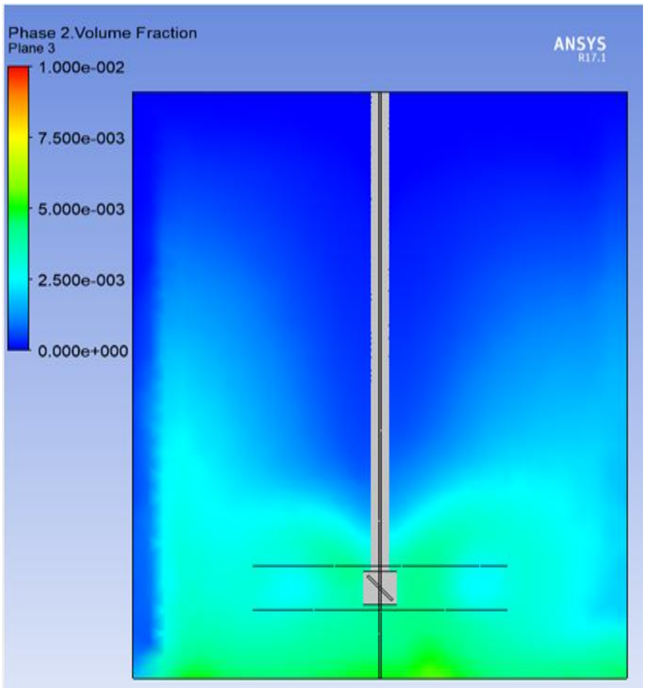

b) Volume fraction distribution of solid particles

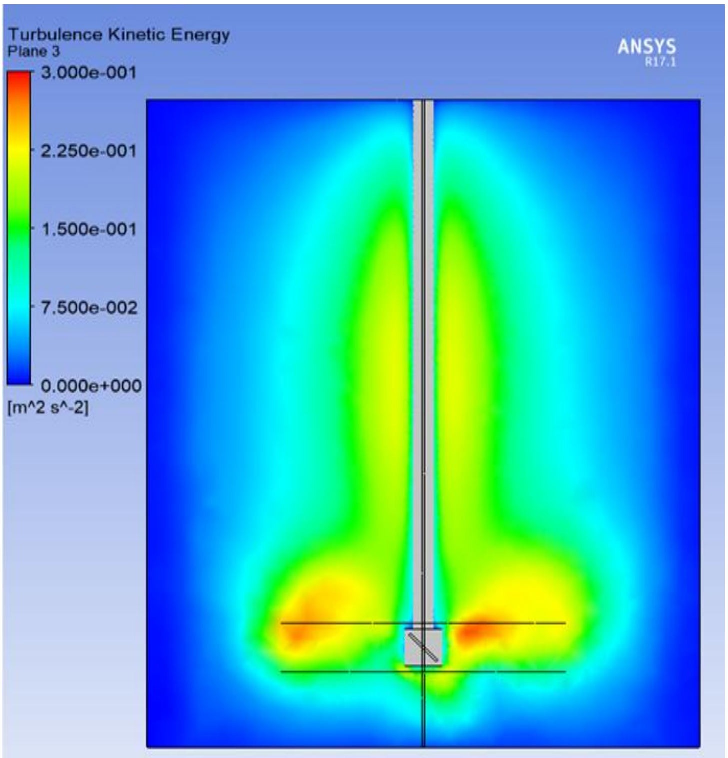

c) Turbulent kinetic energy distribution

Fig 6: Simulation results of counterclockwise rotation of impeller

Here, the downward circulating flow impedes the flow of particles ascending by the impeller, which is redirected by this disturbance and forms a small circulating flow in the downward space. For this reason, the circulating flows formed reduce the overall flow rate and thus the flow distribution becomes nonuniform. Such inhomogeneous phenomena can be clearly seen in Figs. 5 and 6(c).

In Fig. 5c, the maximum turbulent distribution is wider than in Fig. 6c, and the constant turbulent kinetic energy is distributed throughout the stirred tank, and the same result can be qualitatively confirmed through Table 4.

Table 4: Volume-Weight Average Velocity (m/s) along the direction of the impeller rotation

direction of rotation of impeller	volume-weight average velocity
clockwise direction	0.79
counterclockwise direction	0.65

The simulation results show that it is reasonable to choose the direction of rotation that is clockwise, i.e., the direction of rotation that is formed in a push-off manner rather than in a pumping state of fluid flow.

3.2 Effect Of Impeller Position On The Flotation Characteristics And Stirring Effect Of Solid Particles

The simulation was performed by varying the distance between the stirred bed and the impeller bed to determine the distance between the rational impeller and the stirred bed.

In the simulation, the rotational speed was set at 120 rpm and the stirred tissue diameter and the blade diameter ratio was fixed at 0.4.

Table 5 shows the different geometric settings.

Table 5: Selected geometry

Condition parameter	1	2	3
C	0.1H	0.15H	0.2H

As shown in Fig. 7, it can be seen that the volume distribution of the particles in condition 2 is relatively uniform over that of condition 1 and 3, while the concentration concentration phenomenon occurs locally in conditions 1 and 3. In Fig. 8, the velocity distribution of condition 1 is smaller than that of condition 2, and in condition 3 there is a region of weak velocity at the lower stage of the blade. The values of the particle volume-weighted average velocity and maximum velocity versus blade position are listed in Table 6. The simulation results are shown in Figs. 7 and 8.

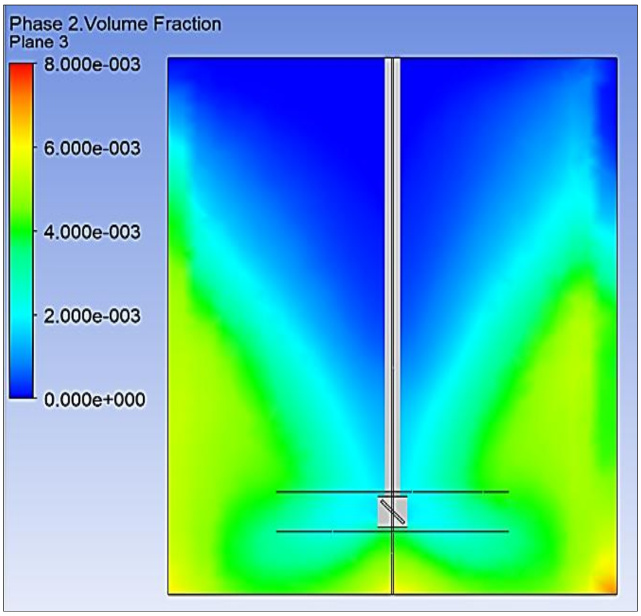

a) Conditon 1

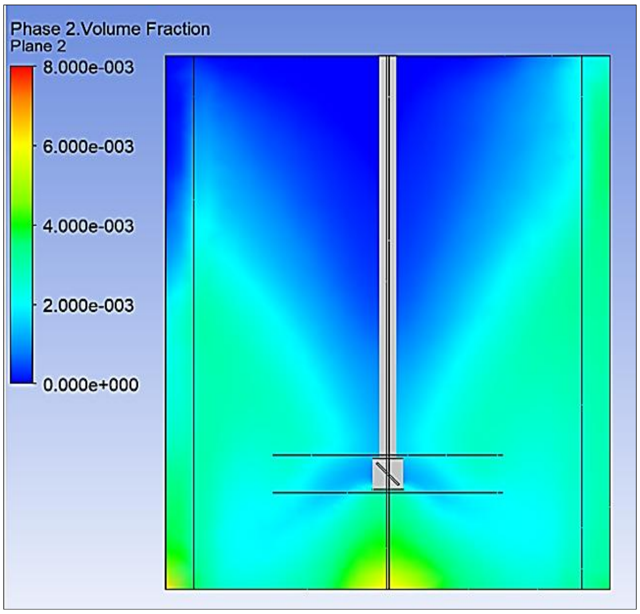

b) Condition 2

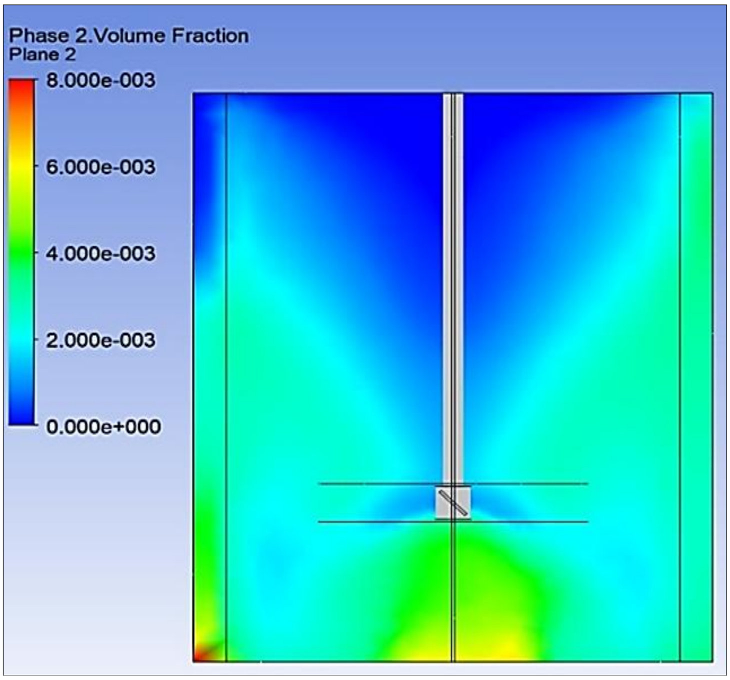

c) Condition 3

Fig 7: Volume distribution of mineral particles under different installation conditions

Table 6: The particle volume-weighted average velocity and maximum velocity (m/s) along the blade position

Mounting position	Volume-weighted average velocity	Maximum velocity
Condition 1	0.220	4.69
Condition 2	0.226	5.56
Condition 3	0.210	4.89

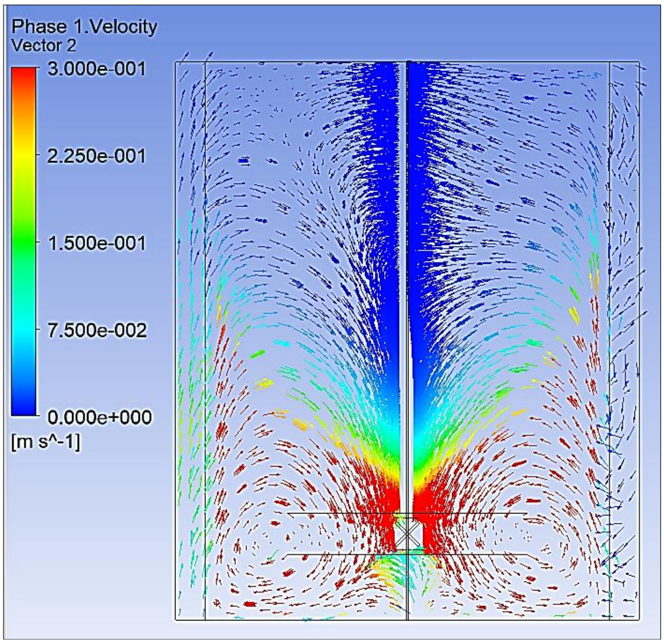

1) Condition 1

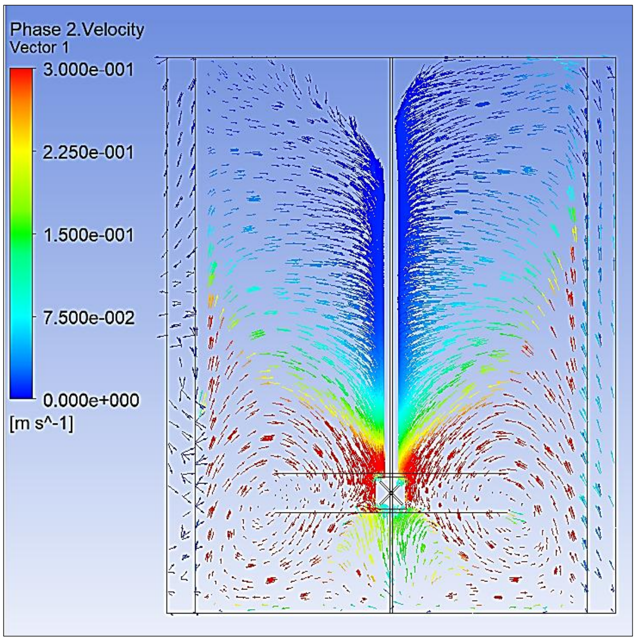

2) Condition 2

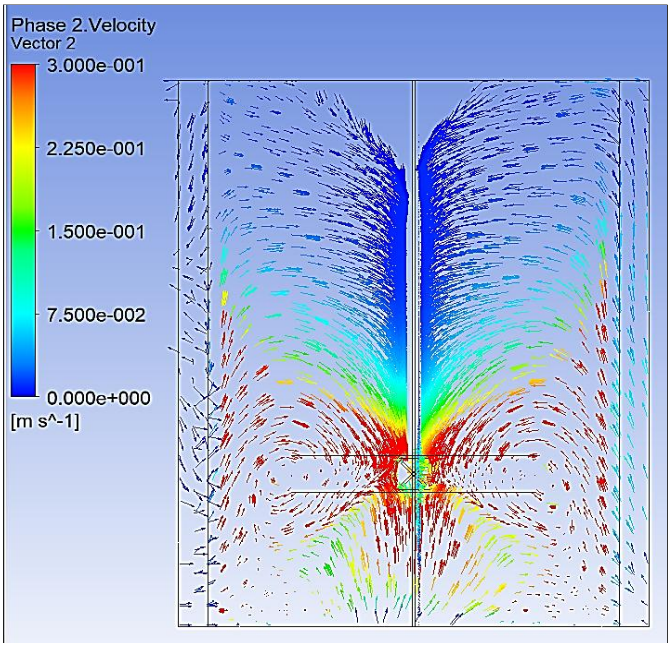

c) Condition 3

Fig 8: Variation of velocity vector with different installation conditions

From the results of Figs. 7, 8 and Table 5, the optimum blade position was chosen as condition 2, i.e. C = 0.15H.

3.3 Effect Of Stirring Speed On The Flotation Characteristics And Stirring Effect Of Solid Particles

Simulations were performed with varying stirring speed to set a reasonable stirring speed. The rotation direction is clockwise and the position of the setup is fixed as "condition 2". Table 7 gives the stirring speeds.

Table 7: Stirring speed

Condition / Parameter	1	2	3
R, r/min	90	120	150

The simulation results are shown in Fig. 9.

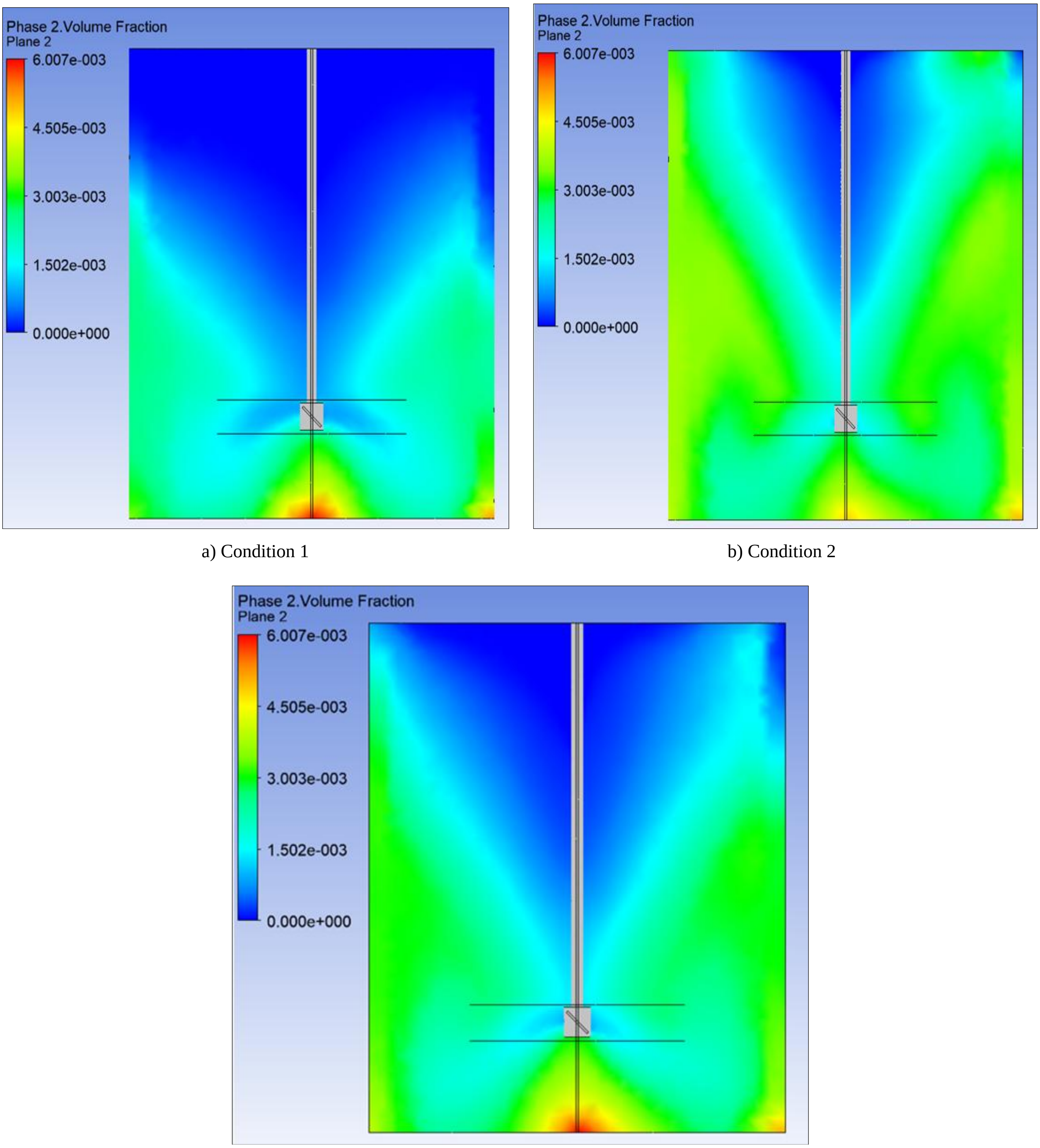

a) Condition 1 b) Condition 2

c) Condition 3

Fig 9: Results of solid volume fraction versus stirring speed

As shown in Fig. 9, it can be seen that the particles are uniformly distributed with increasing stirring speed. This is because the higher the stirring speed, the greater the kinetic energy the particle receives. Vorticity estimation was performed to see the distribution and swirl formation of solid particles.

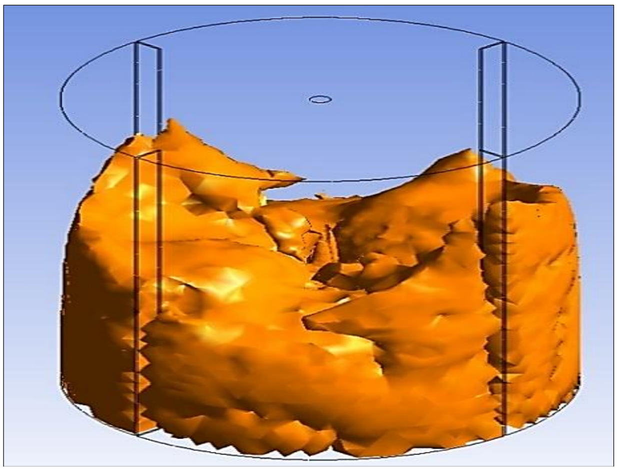

a) Condition 1

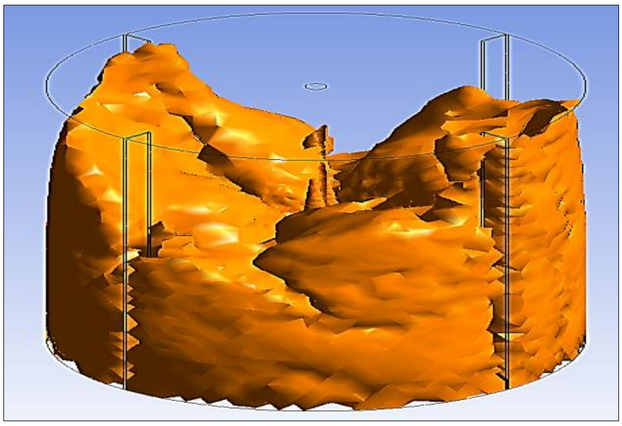

b) Condition 2

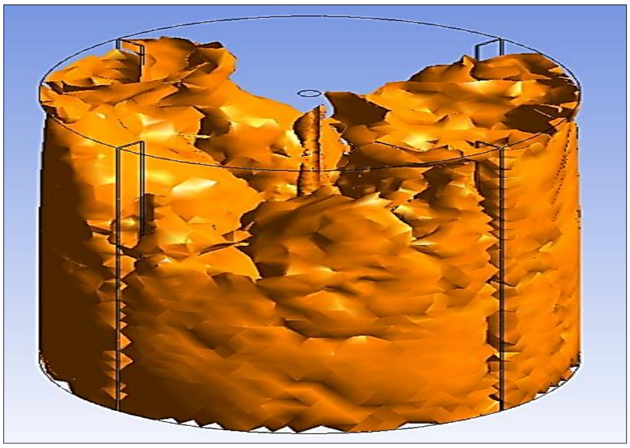

c) Condition 3

Increasing the stirring speed favors the stirring effect, whereas the energy consumption increases. As can be seen in Fig. 9c and c, it can be seen that the particles are relatively uniformly distributed in the whole space of the stirred tank at 150 rpm stirring speed. Therefore, considering the energy consumption and the distribution of solid particles, a reasonable stirring speed of 150 rpm was chosen. From the above simulation results, based on the material balance calculations and CFD simulation results in zinc wet smelting process treating zinc sublimate, the optimum design index of dechlorination stirrer for maximizing the efficiency of cupric chloride precipitation reaction is as follows:

Table 8: Optimal Design Indicator of a Dechlorination Stirrer

Índex		Value	Unit
Leaching tank	diameter	1.0	m
	height	1.5	m
Baffle	Number of baffles	4	
	width	0.2	m
	height	0.9	m
	thickness	10	mm
Agitator blade	diameter	400	mm
	Number of blades	2	
	Number of stages	1	stage
	Diameter of axis	60	mm
	Tilted angle	45	°
	Height between the blade and the bottom of the tide	0.225	m
	Rotation speed	150	r/min
	Rotation direction	Clockwise	

4. Conclusión

In this paper, we have characterized the dispersion characteristics of solid particles in liquid, and based on this, we have carried out a hydrodynamic analysis to determine the optimum structure and size of dechlorination stirrer which can maximize the efficiency of the precipitation reaction. First, a mathematical model was developed to simulate the stirring process in the presence of two phases, liquid and solid. Prior to performing hydrodynamic analysis, in order to study the liquid-solid phase interaction for stirring, the stirring process is the interaction of liquid and solid, and the gas phase interaction such as air and gas generation is neglected, and the chemical reaction is not considered considering the stability and time of solution during stirring. And the fluid flow was considered turbulent because of incompressibility and high Reynolds number, and the small size inside the particle was assumed to be the absence of diffusion-induced heat and mass transfer. Based on the previous studies, governing equations, viscosity equations, turbulent dissipation force models and interface resistance equations were selected. Next, a geometric model of the dechlorination stirrer was constructed using Solidworks and Ansys Fluent was used to investigate the effect of various factors on the flotation characteristics of particles in neutral solution. First, simulations of the impeller rotating clockwise and counterclockwise directions were carried out to investigate the change in volume fraction and turbulent kinetic energy, and on this basis, it was found that the effect was better when the impeller was clockwise. In addition, the impeller was installed at different heights to ensure a reasonable installation position through the variation of volume fraction and turbulent kinetic energy with height. The stirring process with different speeds of the blade was simulated to determine the optimum rotational speed. The above simulation results were combined to identify the optimum design parameters of dechlorination stirrer that can maximize the efficiency of the precipitation reaction.

References

1. Wadnerkar D, Utikar RP, Tade MO, Pareek VK. *CFD* simulation of solid-liquid stirred tanks. Advanced Powder Technology. 2012;23(4):445-453.
2. Kasat GR, Khopkar AR, Ranade VV. *CFD* simulation of liquid-phase mixing in solid-liquid stirred reactor. Chemical Engineering Science. 2008;63:3877-3885.

3. Deglon DA, Meyer CJ. *CFD* modelling of stirred tanks: Numerical considerations. Minerals Engineering. 2006;19(10):1059-1068.
4. Cashman RSM, Harlamovs JR, Dreisinger DB, *et al*. Solvent extraction of a halide from an aqueous sulphate solution. US Patent 0179991A1[P]. 2004-09-16.
5. Cinar Sahin F, Derin B, Yücel O. Chloride removal from zinc ash. Scandinavian Journal of Metallurgy. 2000;29(5):224-230.
6. Güresin N, Topkaya YA. Dechlorination of a zinc dross. Hydrometallurgy. 1998;49(1-2):179-187.
7. Gerald LB, Verner BS, Nicolaus Z. Removal of manganese and chloride ions from aqueous acidic zinc sulphate solutions. US Patent 4379037[P]. 1983-04-05.
8. Haque KE. Microwave energy for mineral treatment processes—a brief review. International Journal of Mineral Processing. 1999;57(1):1-24.
9. Kingman SW, Rowson NA. Microwave treatment of minerals—a review. Minerals Engineering. 1998;11(11):1081-1087.
10. Sigmund PF, Jaakko IP. Hydrometallurgical method for treating valuable metal raw materials containing chlorides and fluorides. US Patent 4698139[P]. 1987-10-06.
11. Qi N, Zhang H. *CFD* simulation of particle suspension in a stirred tank. Particuology. 2013;11:317-326.
12. Sivashanmugam P, Prabhakaran S. Simulation of the effect of baffle length on power consumption in an agitated vessel. International Journal of Food Engineering. 2008;4(2):1-16.
13. Qi NN, Wang H, Zhang K, Zhang H. Numerical simulation of fluid dynamics in the stirred tank by the SSG Reynolds stress model. Frontiers of Chemical Engineering in China. 2010;4(4):506-514.
14. Khopkar AR, Kasat GR, Pandit AB, Ranade VV. Computational fluid dynamics simulation of the solid suspension in a stirred slurry reactor. Industrial & Engineering Chemistry Research. 2006;45(12):4416-4428.
15. Deglon DA, Meyer CJ. *CFD* modeling of stirred tanks: Numerical considerations. Minerals Engineering. 2006;19(10):1059-1068.
16. Ochieng A, Lewis AE. *CFD* simulation of nickel solids concentration distribution in a stirred tank. Minerals Engineering Journal. 2006;19:180-189.
17. Fajner D, Magelli F, Nocentini M, Pasquali G. Solids concentration profiles in a mechanically stirred, staged column slurry reactor. Chemical Engineering Research and Design. 1985;63:235-240.
18. Ochieng A, Onyango MS, Kumar A, Kiriamiti HK, Musonge P. Mixing and power draw in a tank stirred by a *Rushton* turbine at a low clearance. Chemical Engineering and Processing Journal. 2008;47(5):842-851.
19. Pukkella AK, Vysyaraju R, Tammishetti V, Rai B, Subramanian S. Improved mixing of solid suspensions in stirred tanks with interface baffles: *CFD* simulation and experimental validation. Chemical Engineering Journal. 2018;1:1-10.
20. Wadnerkar D, Tade MO, Pareek VK, Utikar RP. *CFD* simulation of solid-liquid stirred tanks for low to dense solid loading systems. Particuology. 2016;29:16-33.a